Fast Compressed Sensing SAR Imaging Based on Approximated Observation

Jian Fang, *Student Member, IEEE*, Zongben Xu, Bingchen Zhang, Wen Hong, *Member, IEEE*, and Yirong Wu, *Member, IEEE*

***Abstract*—In recent years, compressed sensing (CS) has been applied in the field of synthetic aperture radar (SAR) imaging and shows great potential. The existing models are, however, based on application of the sensing matrix acquired by the exact observation functions. As a result, the corresponding reconstruction algorithms are much more time consuming than traditional matched filter (MF)-based focusing methods, especially in high resolution and wide swath systems. In this paper, we formulate a new CS-SAR imaging model based on the use of the approximated SAR observation deducted from the inverse of focusing procedures. We incorporate CS and MF within an sparse regularization framework that is then solved by a fast iterative thresholding algorithm. The proposed model forms a new CS-SAR imaging method that can be applied to high-quality and high-resolution imaging under sub-Nyquist rate sampling, while saving the computational cost substantially both in time and memory. Simulations and real SAR data applications support that the proposed method can perform SAR imaging effectively and efficiently under Nyquist rate, especially for large scale applications.**

***Index Terms*—Approximated observation, compressed sensing, matched filtering, synthetic aperture radar.**

I. Introduction

SYNTHETIC aperture radar (SAR) is an active microwave radar that can achieve high-resolution images in all times of day and weather [1]. In an SAR system, the radar emits a sequence of pulses along its path and receives the echoes (raw data) scattered from the targets. The reconstruction of the scene is traditionally achieved by matched filter (MF)-based focusing algorithms that are efficient but need Nyquist rate samples of the echoes. The SAR imaging with increasing resolution and swath requires more and more measurements, storage, and downlink bandwidth. The current system hardware, however, frequently hampers such high-dimensional application.

The recent development of compressed sensing (CS) brings the possibility of reconstructing sparse or compressible signals with fewer measurements than that Nyquist requires [2][3][4]. Several applications on radar system appear in recent years, which primarily concern how the data acquisition procedure can be simplified by using CS [5], [6] and what the potential applications will renovate radar imaging with CS technique [7], [8]. Further, in the study of CS-SAR, much attention has been paid to the effective use of the specific SAR geography and signal form, say, in [9], an SAR raw data compression framework based on CS was suggested by sampling the data in frequency domain. An extension of this work was given in [10] by using the fact that very bright objects are always sparse, resulting in a hybrid sparse model. These works, however, do not apply to the CS-SAR system practically where sampling is expected in time-domain. In [11], CS was applied on azimuth after the range compression. By combining range MF, the method was much more efficient, while, the redundant information in range has not been effectively utilized. More general CS-SAR model were reported in [12], [13] by discretizing the SAR observation function exactly into an observation matrix, while solving by CS straightforwardly.

All those works strongly demonstrated that some exclusive advantages of CS-SAR do exist as compared with the traditional SAR imaging methodologies, say, relaxation of required measurements, reduction of sidelobe, and a further suppression of noise [14]. However, in all applications, a serious drawback has been observed: as compared with the traditional MF-based methods, the computational complexity and memory cost of the CS-SAR models are much higher so that it is very inefficient to be applied to high-dimensional applications.

In this paper, we formulate a new CS-SAR framework within which the computational complexity of the CS-SAR imaging can be significantly reduced. Our main idea is to replace the exact observation function in the CS-SAR framework with approximated observations derived from the inverse of traditional MF based procedures. Such inversion has always been applied to yield raw signals (the echoes) in a more economical way [15], [16] but requires high accuracy of the adopted method. In this paper, we take a further step by incorporating it into the CS framework, which demands only a well-focusing ability to ensure CS reconstruction. We propose to implement the CS-SAR imaging through the sparse regularization scheme, which is then solved by an iterative thresholding algorithm (ITA). Accordingly, the fast speed and high efficiency of the new method are guaranteed, respectively, from the use of the approximated observation and from the CS reconstruction procedure. We show that the new CS-SAR imaging method can not only acquire high-quality and high-resolution images with significantly reduced measurements, but also reduces the memory cost to $\mathcal{O}(n)$ and computational complexity of one-step iteration to $\mathcal{O}(n \log n)$, achieving the same order with the traditional SAR imaging methods.

The reminder of the paper is organized as follows. In Section II, we introduce the background knowledge on the

Manuscript received January 01, 2013; revised April 01, 2013; accepted May 01, 2013. Date of publication May 31, 2013; date of current version December 18, 2013. This work was supported by the State Key Development Program for Basic Research of China (973 Program) (Grant 2010CB731905), National Natural Science Foundations of China (Grant 11131006) and the National Natural Science Foundations of China (Grants 61075054, 60975036, 11171272).

J. Fang and Z. Xu are with the School of Mathematics and Statistics, Xi'an Jiaotong University, Xi'an 710049, China (e-mail: zbxu@mail.xjtu.edu.cn).

B. Zhang, W. Hong, and Y. Wu are with the Institute of Electronics, Chinese Academy of Sciences, Beijing 100190, China.

Color versions of one or more of the figures in this paper are available online at http://ieeexplore.ieee.org.

Digital Object Identifier 10.1109/JSTARS.2013.2263309

stripmap mode SAR system and the classical CS-SAR model. In Section III, we present the approximated observation by calculating the inverse of MF imaging procedure. In Section IV, we formulate the new CS-SAR imaging method through hybridizing the approximated observation and sparse regularization. In Section V, we show the simulation and application results of the suggested method. Conclusions are then presented in Section VI with some useful remarks.

Notation: We will use the subsequent notations throughout the paper: Column vectors, matrices, and operators will be denoted, respectively, by bold lower case, $\mathbf{x}$, bold upper case, $\mathbf{A}$, and roman upper case, C. $\mathbf{A^T}$, $\mathbf{A}^*$, and $\mathbf{A^H}$ denote the transpose, conjugate, and Hermitian transpose of $\mathbf{A}$, respectively.

II. CS-SAR Models Based on Exact Observation

In this section, some preliminary knowledge of CS-SAR imaging is summarized. We focus on the general formalization of CS-SAR model, with a more detailed introduction of the iterative thresholding procedures for solution of the CS-SAR models.

A. Stripmap Mode SAR Model

In the stripmap mode SAR, the antenna is pointed to a fixed direction and the platform flights with constant velocity v. Then, a complex baseband $p_c(\tau)$, usually chirp, is modulated to real pulse $p(\tau) = \cos(2\pi f_0\tau + \phi(\tau))(-(t_s/2) \le \tau \le (t_s/2))$ (f_0 is the carrier frequency, τ is the range time, and t_s is the pulse duration) and is transmitted at a constant pulse repetition frequency (PRF). The received backscattered energy can then be modeled as a convolution of the pulse waveform with the ground reflectivity function. More specifically, the received echoes s at time (η', τ') can be expressed by

$$s(\eta', \tau') = \int\int \sigma(\eta, \tau) g(\eta' - \eta, \tau'; \tau) d\eta d\tau + n_0(\eta', \tau') \quad (1)$$

where

$$g(\eta' - \eta, \tau'; \tau) = \omega_\eta(\eta' - \eta)\omega_\tau\left(\tau' - \frac{2R}{c}\right)\exp\left[-\frac{4\pi R}{\lambda} + \phi\left(\tau' - \frac{2R}{c}\right)\right], \quad (2)$$

λ is the carrier wavelength, c is the velocity of light, ω is the envelope function, $R(\eta' - \eta; \tau) = \sqrt{(\tau c/2)^2 + [v(\eta' - \eta)]^2}$ is the slant range, $n_0(\eta', \tau')$ is the complex Gaussian noise.

Further, we can sample the continuous-time analog echo s and discrete the reflectivity map σ, into two-dimensional arrays $\mathbf{Y} \in \mathbb{C}^{n'_\eta \times n'_\tau}$ and $\mathbf{X} \in \mathbb{C}^{n_\eta \times n_\tau}$. And then we obtain the following observation model for the strip mode SAR:

$$\mathbf{y} = \mathbf{H}\mathbf{x} + \mathbf{n}_0 \quad (3)$$

where $\mathbf{y} = \mathrm{vec}(\mathbf{Y}) \in \mathbb{C}^{l \times 1}$, $l = n'_\eta \times n'_\tau$, $\mathbf{x} = \mathrm{vec}(\mathbf{X}) \in \mathbb{C}^{n \times 1}$, $n = n_\eta \times n_\tau$, and $\mathbf{H}$ is the observation matrix acquired from the discrete weight of (1) (more detailed information and construction of the observation model can be seen in [17] and [18]), and $\mathbf{n}_0$ is the noise.

Algorithm 1: Soft Iterative Thresholding Algorithm

Require: Measurements $\mathbf{y}_s$, sensing matrix $\mathbf{A}$
Ensure: The recovery signal $\mathbf{x}$
Initial: $\mathbf{x}^{(0)}$, λ, μ and max iteration $I_{\max}$
1: **for** $i = 0$ to $I_{\max}$ **do**
2: Gradient descent step: $\mathbf{g}^{(i+1)} = \mathbf{x}^{(i)} + \mu\mathbf{A}^{\mathrm{T}}(\mathbf{y}_s - \mathbf{A}\mathbf{x}^{(i)})$
3: Thresholding: $\mathbf{x}^{(i+1)} = \mathrm{E}_{1,\lambda\mu}(\mathbf{g}^{(i+1)})$
4: **end for**

B. Formulation of CS-SAR Models

In a CS-SAR model, the data $\mathbf{y}$ is sampled and compressed with a proper sampling matrix $\mathbf{\Theta} \in \mathbb{R}^{m \times l}$, $m \ll n$, resulting in

$$\mathbf{y}_s = \mathbf{\Theta}\mathbf{H}\mathbf{x} + \mathbf{n}_s. \quad (4)$$

When $\mathbf{x}$ is a sparse signal, say, most of the entries of $\mathbf{x}$ are zeros, the theory of CS tells when and how it can be recovered from the above undetermined linear system with fewer measurements than Nyquist criterion requires [2], [4]. Generally, considering an ill-posed linear system $\mathbf{y}_s = \mathbf{A}\mathbf{x}$ ($\mathbf{A} = \mathbf{\Theta}\mathbf{H}$), where $\mathbf{x}$ is sparse enough, if the sensing matrix $\mathbf{A}$ satisfies some conditions like RIP [19], $\mathbf{x}$ can be exactly recovered from $\mathbf{y}_s$ with the L_q (quasi-norm) $(0 \le q \le 1)$ optimization:

$$\min_{\mathbf{x}} \quad \|\mathbf{x}\|_q \quad \text{s.t.} \quad \mathbf{y}_s = \mathbf{A}\mathbf{x}. \quad (5)$$

To solve (5), one may use the interior point method and greedy strategies like OMP. However, they always require deeper information of $\mathbf{A}$ that are not suitable for the to be established problem. As an alternative, we suggest use of an equivalent regularization scheme with the following optimization problem:

$$\min_{\mathbf{x}} \quad \left\{\|\mathbf{y}_s - \mathbf{A}\mathbf{x}\|_2^2 + \lambda\|\mathbf{x}\|_q^q\right\} \quad (6)$$

where λ is a regularization parameter. The optimization can be efficiently solved by iterative thresholding algorithm (ITA) [20], [21], [22]. In detail, an ITA generates a sequence of approximates according to

$$\mathbf{x}^{(i+1)} = \mathrm{E}_{q,\lambda\mu}\left(\mathbf{x}^{(i)} + \mu\mathbf{A}^{\mathrm{H}}\left(\mathbf{y}_s - \mathbf{A}\mathbf{x}^{(i)}\right)\right) \quad (7)$$

where μ is a normalized parameter that controls the convergence of the iteration. In (7), $\mathrm{E}_{q,\sigma}$ ($\sigma = \lambda\mu$) is a so-called thresholding operator, which is defined in terms of components by

$$\mathrm{E}_{q,\sigma}(\mathbf{x}) = (e_{q,\sigma}(\mathbf{x}_1), e_{q,\sigma}(\mathbf{x}_2), \ldots e_{q,\sigma}(\mathbf{x}_n))^{\mathrm{T}} \quad (8)$$

where $e_{q,\sigma}$ can be analytically specified when $q = 0, 1/2, 2/3, 1$. For example, the widely used soft-thresholding, which corresponds to $q = 1$, is

$$e_{1,\sigma}(x) = \begin{cases} \mathrm{sgn}(x)(|x| - \sigma), & \text{if } |x| \ge \sigma \\ 0, & \text{otherwise.} \end{cases} \quad (9)$$

With (7) and (8), ITA can be viewed as an extension of the gradient descent method by introducing a thresholding procedure in each step. The detail implementation of the standard soft thresholding can be seen in Algorithm 1.

It can be seen that the main computation load in implementation of (7) comes from the calculation of the time-domain correlation $\mathbf{A}^{\mathrm{H}}\mathbf{A}\mathbf{x}$. From the viewpoint of SAR signal processing, this corresponds to the backscattered projection procedure, which is known to be inefficiency for reconstruction, even implemented by convolution as in (1). On the other hand, we notice that there exists efficient focusing methods using MF in traditional SAR signal processing. This type of processing is in the frequency domain, which is much faster. Moreover, unlike the MF-based method which is usually decoupled, the sensing matrix $\mathbf{H}$ in (7) owns an intrinsically two-dimensional structure that has to be collected and stored before imaging. Although some compression can be incorporated according to the structure of the matrix, it still consumes a huge memory. All these difficulties then hamper effective applications of the known CS-SAR imaging.

The aim of the present research is to suggest a new CS-SAR imaging method, which replaces the use of the exact observation model by an well-defined approximation, and then makes it possible to reconstruct the sparse scene $\mathbf{x}$ via a sequence of 1-D operations. Thus, the very high cost of calculation and memory of the existing CS-SAR imaging methods can be significantly reduced.

III. Approximated Observation

In this section, we first explain why an approximated observation is needed and feasible, and then we provide an example to show how an approximated observation operator can be explicitly constructed by virtue of a concrete example from the inverse of the Range-Doppler Algorithm (RDA). A relation between the constructed approximation and the corresponding focus method is analyzed, which then serves as the basis of the development of new method in the next section.

A. Why Approximation Needed

It is known that MF is fast with $\mathcal{O}(n\log n)$ complexity, which is, among the others, mainly due to frequency-domain operations. More precisely, if we denote $\mathbf{M}$, the imaging procedure by MF, like RDA, the SAR raw data can be well focused in some conditions by

$$\tilde{\mathbf{x}} = \mathbf{M}\mathbf{y} \tag{10}$$

where $\mathbf{M}$ is the traditional MF imaging procedure that can be calculated through decoupling it into a series of 1-D operators in the frequency domain. This normally leads to an $\mathcal{O}(n\log n)$ complexity when fast Fourier transformation (FFT) type operations are employed.

Observing these advantages, the purpose of this paper is to accelerate the known CS-SAR imaging procedures so as to achieve a comparable (at the same order) complexity with the traditional MF based methods.

A natural consideration is then to look for the possibility of integrating CS and MF. However, a direct application on the decoupling of $\mathbf{H}$ is impossible, because $\mathbf{H}$ intrinsically possesses 2-D structure. Nevertheless, it is known from (10) that $\tilde{\mathbf{x}}$ always approximates $\mathbf{x}$, say, $\mathbf{M}\mathbf{H} \approx \mathbf{I}$, and hence, $\mathbf{M}^{-1}$, whenever it exists, approximates the observation $\mathbf{H}$. In viewing that $\mathbf{M}$ is decoupled, it can then naturally be expected that $\mathbf{M}^{-1}$ is decoupled, as well. Thus, we can expect that under certain conditions, some types of approximations of $\mathbf{H}$ can be decoupled so as to bring an $\mathcal{O}(n\log n)$ complexity.

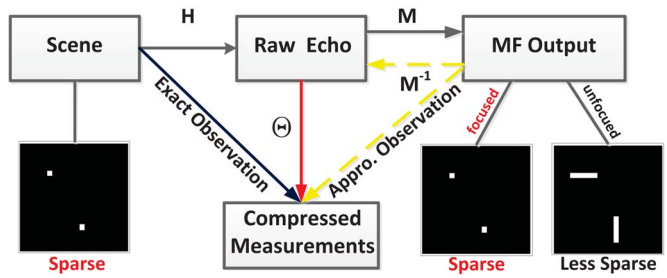

Fig. 1. Relations between exact observation and approximated observation.

This is why we would like to approximate the observation, and in the following, we will introduce the details on how to construct and what constraints an appropriate approximation observation.

B. How to Construct an Admissible Approximated Observation

Fig. 1 draws the main relations between CS-SAR observation and MF reconstructions. It can be seen that whenever the imaging procedure $\mathbf{M}$ is accurate enough, $\mathbf{M}^{-1}$ can be viewed as an admissible substitute of $\mathbf{H}$. This provides a general principle of how the observation $\mathbf{H}$ can be remodeled and approximated by any high-precision imaging (or reconstruction) procedure. We formalize this principle further as

$$\mathbf{G} = \mathbf{M}^{-1} \approx \mathbf{H} \tag{11}$$

where $\mathbf{G}$ is any generalized right inverse of $\mathbf{M}$, and $\mathbf{M}$ is any a high-precision imaging procedure. We call $\mathbf{G}$ henceforth an *approximated observation*.

However, since there are many well-known imaging procedures that provided various tradeoffs on imaging accuracy and complexity. Therefore, we need to further define the extent of accuracy and identify the constraints under the CS-SAR framework. To see this, let us compare the exact observation model and the approximated observation model:

$$\mathbf{y}_s = \mathbf{\Theta}\mathbf{H}\mathbf{x} = \mathbf{\Theta}\mathbf{G}\tilde{\mathbf{x}}. \tag{12}$$

It can be seen that by using approximated observation, other than reconstruct $\mathbf{x}$, we actually reconstruct $\tilde{\mathbf{x}}$ instead, which is assumed to be an approximation of $\mathbf{x}$, when it obeys to the following relation:

$$\tilde{\mathbf{x}} = \mathbf{p}_\epsilon \circ \mathbf{x} + \mathbf{s}_\epsilon \tag{13}$$

where $\circ$ denotes the Hadamard product, $\mathbf{p}_\epsilon$ denotes the phase error while $\mathbf{s}_\epsilon$ is the error for sidelobe or, more severely, the artifacts from unfocusing. Formally, when (13) holds, there exists an acceptable solution with the approximated observation model. However, to find it under CS, we should further emphasize the better focusing ability of $\mathbf{M}$.

As we know, a key parameter in CS-SAR, different from traditional SAR, is the sampling rate that measures how an SAR

system benefits from CS. The least amount of samples to ensure the reconstruction is incoherently determined by the sparsity of scene $\mathbf{x}$, which is usually irrelevant of the distribution and phases of targets in the scene. Thus, the difference of the sparsity between $\mathbf{x}$ and $\tilde{\mathbf{x}}$ determines when and how much of the additional measurements do the approximated observation-based CS-SAR methods need. It can be immediately seen from (13) that the difference is uniquely characterized via $\mathbf{s}_\epsilon$. That is to say, whenever the sidelobes reconstructed from $\mathbf{M}$ is low enough, $\mathbf{s}_\epsilon$ can be ignored, then $\mathbf{x}$ and $\tilde{\mathbf{x}}$ can keep the same sparsity. In this situation, the required least sampling rate of the approximated observation model equals the original model. In turn, to prevent the approximated observation-based CS-SAR method from demanding more samples, the sidelobe should be as low as possible, or, equivalently, a well-focused capacity should be a criterion to determine whether a specific focusing method can be used to construct the approximated observation.

The above discussions relate the fact that the construction of the approximated observation is quite reflexible, which can be acquired straightforwardly based on well-established algorithms with additional requirement on the focusing ability. In Section III-C, we present a concrete example using Range-Doppler-algorithm (RDA)[23] to show how an admissible approximated observation $\mathbf{G}$ can be simply constructed based on this principle.

C. A Concrete Example

RDA is a very popular procedure for stripmap mode SAR imaging that is simple both in comprehension and in implementation. The procedure (under the low squint case) consists of three main steps (operations): 1) the range compression, 2) RCMC, and 3) azimuth compression. In a compact form, the imaging procedure M, operated on 2-D array, can then be expressed as follows:

$$\tilde{\mathbf{X}} = \mathrm{M}(\mathbf{Y}) = \mathbf{F}_\eta^{\mathrm{H}} \left\{ \mathbf{P}_\eta \circ \mathrm{C} \left\langle \mathbf{F}_\eta \left[\mathbf{P}_\tau \circ (\mathbf{Y}\mathbf{F}_\tau) \right] \mathbf{F}_\tau^H \right\rangle \right\} \quad (14)$$

where $\tilde{\mathbf{X}}$ ($\tilde{\mathbf{x}} = \mathrm{vec}(\tilde{\mathbf{X}})$) is the reconstructed 2D SAR image, $\mathbf{F}$ and $\mathbf{F}^{\mathrm{H}}$, respectively, are the DFT matrix and inverse DFT matrix (in practice, they are implemented by FFT) to perform, the subscripts η and τ denote the direction of azimuth and range where the FFT performs along, and $\mathbf{P}_\eta$ and $\mathbf{P}_\tau$ are the frequency-domain matched filter operations along azimuth and range, which can be always defined, respectively, by

$$\mathbf{P}_\eta(f_\eta;\tau) = \exp\left[-j\pi/K_a f_\eta^2\right] \quad \mathbf{P}_\tau(f_\tau) = \exp\left[-j\pi/K_r f_\tau^2\right]. \quad (15)$$

In (15), f_η, f_τ are the frequency along the Doppler and range, and K_a and K_r are the azimuth FM rate and the pulse FM rate. In (14), C is the RCMC interpolation operator, which is essentially a space-variant shift and is always approximated by the truncated sinc-kernel interpolation with $\mathbf{U} = \mathrm{C}(\mathbf{V})$ as

$$\mathbf{U}(f_\eta,\tau) = \sum_{\tilde{\tau}} \mathbf{V}(\tilde{f}_\eta,\tilde{\tau})\mathrm{sinc}(\tilde{\tau} - (\tau + \Delta r(f_\eta,\tau)) \quad (16)$$

where Δr is the migration (measurement in time) to be corrected, and $\mathbf{U}$ and $\mathbf{V}$ are the signals before and after RCMC, respectively.

With such specific operations in RDA procedure, we now can derive the inverse of $\mathbf{M}$ quite simply by taking the inverse of every subprocedure. The details are as follows.

i) The inverse of Fourier transformations $\mathbf{F}, \mathbf{F}^{\mathrm{H}}$ are known as the inverse transformations, which are given by $\mathbf{F}^{\mathrm{H}}, \mathbf{F}$. It is important to keep the throw-away consistent between the pairs.

ii) It is known that phase multiplication is a unitary transformation so that the inverse is the multiplication of the conjugate phase $\mathbf{P}_\eta^*, \mathbf{P}_\tau^*$, and the Hadamard multiplication can still be applied in order.

iii) The inverse of C is difficult to achieve directly. In fact, C is approximated from the accurate RCMC defined in a continuous range time domain. Because the trajectories of targets with different range gates are disjoint, this shift is a one-to-one mapping, and the inverse of the origin RCMC exists. We can also approximate through interpolation $\mathbf{V} = \mathrm{D}(\mathbf{U})$ that

$$\mathbf{V}(\tilde{f}_\eta,\tilde{\tau}) = \sum_{\tau} \mathbf{U}(f_\eta,\tau)\mathrm{sinc}(\tilde{\tau} - (\tau + \Delta r(f_\eta,\tau))). \quad (17)$$

Based on the above exposition, the approximated observation G deduced from RDA can then be explicitly expressed by

$$\mathrm{G}(\mathbf{X}) = \left\{ \mathbf{P}_\tau^* \circ \left\langle \mathbf{F}_\eta^{\mathrm{HD}} \left[\mathbf{P}_\eta^* \circ (\mathbf{F}_\eta \mathbf{X}) \right] \mathbf{F}_\tau \right\rangle \right\} \mathbf{F}_\tau^H. \quad (18)$$

We show that the so-constructed approximated observation $\mathbf{G}$ has an interesting property: It is still a linear operator, and its conjugate transposition equals to $\mathbf{M}$.[1]

Theorem 1: $\mathbf{G}$ is a linear operator with the property $\mathbf{G}^{\mathrm{H}} = \mathbf{M}$.

Proof: The linearity of G and M is obvious because all the suboperations are linear. Let $\mathbf{x}$ denote the vector form of $\mathbf{X}$, namely, $\mathbf{x} = \mathrm{vec}(\mathbf{X})$. Then, by definition, the linear operators G and M can be written as matrices, and we then have

$$\mathrm{vec}\left(\mathrm{G}(\mathbf{X})\right) = \mathbf{G}\mathbf{x} = \hat{\mathbf{F}}_\tau^{\mathrm{H}} \hat{\mathbf{P}}_\tau^* \hat{\mathbf{F}}_\eta^{\mathrm{H}} \hat{\mathbf{F}}_\tau \hat{\mathbf{D}} \hat{\mathbf{P}}_\eta^* \hat{\mathbf{F}}_\eta \mathbf{x} \quad (19)$$

$$\mathrm{vec}\left(\mathrm{M}(\mathbf{Y})\right) = \mathbf{M}y = \hat{\mathbf{F}}_\tau^{\mathrm{H}} \hat{\mathbf{P}}_\eta \hat{\mathbf{C}} \hat{\mathbf{F}}_\eta \hat{\mathbf{F}}_\tau^{\mathrm{H}} \hat{\mathbf{P}}_\tau \hat{\mathbf{F}}_\tau \mathbf{x} \quad (20)$$

where

$$\hat{\mathbf{F}}_\eta = \mathbf{I}_{n_\tau} \otimes \mathbf{F}_\eta, \hat{\mathbf{F}}_\tau = \mathbf{F}_\tau^{\mathrm{T}} \otimes \mathbf{I}_{\mathbf{n}_\eta} \quad (21)$$

$$\hat{\mathbf{P}}_\eta = \mathrm{diag}\left(\mathrm{vec}(\mathbf{P}_\eta)\right), \hat{\mathbf{P}}_\tau = \mathrm{diag}\left(\mathrm{vec}(\mathbf{P}_\tau)\right). \quad (22)$$

$\hat{\mathbf{C}}$ and $\hat{\mathbf{D}}$ are real matrices defined by

$$\begin{cases} \hat{\mathbf{C}}(i,j) = \mathrm{sinc}\left(\frac{j-i}{n_\eta} + \Delta\mathbf{r}(i)/f_s\right) \\ \hat{\mathbf{D}}(i,j) = \mathrm{sinc}\left(\frac{i-j}{n_\eta} + \Delta\mathbf{r}(j)/f_s\right) \end{cases} \quad (23)$$

at locations $(i-j)\mathrm{mod}n_\eta \equiv 0$, and 0 elsewhere. In (23), $\Delta r = \mathrm{vec}(\Delta\mathbf{R})$, $\Delta\mathbf{R}$ is the discretion of Δr. Observing from (23) and f_s is the pulse sampling interval, it is easy to check that $\hat{\mathbf{D}} = \hat{\mathbf{C}}^{\mathrm{T}}$. Consequently, comparing (20) and (19), we conclude that $\mathbf{G} = \mathbf{M}^{\mathrm{H}}$. ■

Theorem 1 shows that we have actually taken the conjugate transposition of $\mathbf{M}$ as an approximated observation of $\mathbf{H}$. Such coincidence plays an important role in the new method to be suggested in the next section.

[1]It is to say $\mathbf{G}$ is nearly unitary, since only a minor approximation on calculation of the inverse is included.

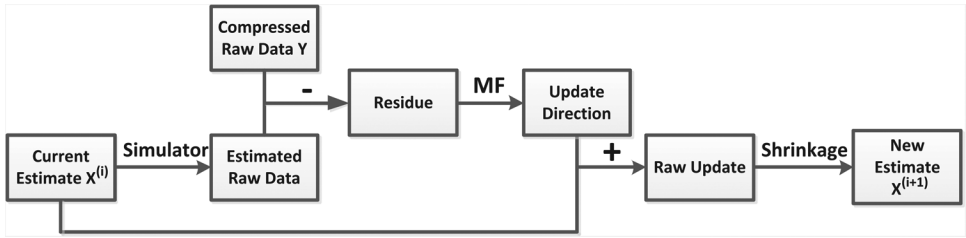

Fig. 2. Explanation of the proposed algorithm in one-step iteration. The compressed data is alternatively processed by MF and thresholding.

D. Generalization

The approach we have applied to define the approximated observation by the inverse of RDA procedure can be generalized in the following.

1) For high-squint cases, we can incorporate secondary compression in RDA or derive an approximated observation from the inverse of other focusing methods like the Chirp-Scaling Algorithm (CSA), $\omega - \mathrm{k}$ algorithms, so as to enhance the focusing ability. With similar suboperations, like FFT, phase multiplication, and interpolation, the acquisition of the inverse is just as same as RDA.
   This principle can be applied to yield more general algorithms; however, we will not enumerate all possible extensions but remind that the decoupled structure of MF makes the inverse always achievable. This is the reason why MF is fast and why we propose to apply the approximated observation instead of the exact observation in the CS-SAR imaging system.
2) In the above derivation, we have assumed that the transmitted signal form is standard chirp and $\mathbf{M}$ focuses on both the azimuth and range direction. In fact, the azimuth modulation is the exclusive property and the main difficulty of SAR signal processing, while the range convolution, which possesses a simple 1-D structure, can be modeled directly. Therefore, we can apply the approximated observation to nonchirp cases, by replacing $\mathbf{P}_\tau^*$ with the transmitted pulse, which is always recorded in modern SAR systems. This extension is also of specific necessity in CS-SAR because the design of the pulse form is also a very important issue.
   Nevertheless, different from the exact observation, which can be discreted from the arbitrary slant range, say, any position during the flight, the construction of approximated observation relies highly on the SAR operation mode and requires uniform samples. This makes the new model more sensitive to the deviation and errors during the flight, and, hence, more suitable in space-borne cases. However, this limitation is not serious, since the goal of the present research is to break the computational burden of large-scale CS-SAR problem. Space-borne cases are just our main target.

IV. CS-SAR Imaging Based on Approximated Observation

In this section, we formulate the new CS-SAR imaging method based on the use of approximated observation. An L_q regularization model, together with the fast iterative thresholding algorithm, will be suggested.

A. New CS-SAR Method

Restricted by the operator form, we could only calculate the conjugate of the approximated observation. Hence, ITA, as seen in (7), is one of the few methods that is suitable to solve this problem. More specifically, by replacing the exact observation $\mathbf{H}$ using the approximated observation G in (18), we can acquire the following CS-SAR model:

$$\min_{\mathbf{X}} \left\{ \|\mathbf{Y}_s - \mathbf{\Theta}_\eta \mathrm{G}(\mathbf{X}) \mathbf{\Theta}_\tau\|_F^2 + \lambda \|\mathbf{X}\|_q^q \right\} \tag{24}$$

where $\|\cdot\|_F$ is the Frobenius norm of a matrix, and $\mathbf{\Theta}_\eta$ and $\mathbf{\Theta}_\tau$ are the sampling operators in azimuth and range directions, which correspond to the general sampling operator $\mathbf{\Theta}$ in (4). It is well defined because the azimuth signal is of discrete form and the range signal is of continuous form, and thus the sampling procedure of the two types of signals are usually physically separated.[2]

Then, due to the linearity of G, the model (24) can still be very fast solved by ITA, which reads in this case that

$$\mathbf{X}^{(i+1)} = \mathrm{E}_{1,\lambda\mu} \left(\mathbf{X}^{(i)} + \mu \mathrm{M} \left(\mathbf{\Theta}_\eta^{\mathrm{T}} \left(\mathbf{Y}_s - \mathbf{\Theta}_\eta \mathrm{G} \left(\mathbf{X}^{(i)} \right) \mathbf{\Theta}_\tau \right) \mathbf{\Theta}_\tau^{\mathrm{T}} \right) \right). \tag{25}$$

In this paper, we simply select $q = 1$ while parameters μ, λ will be preset according to the next subsection.

Fig. 2 below shows the flowchart of algorithm (25), which tells that ITA provides an intuitive explanation in terms of SAR signal processing. It is seen that at each iteration, the ITA can be decomposed into mainly three procedures: 1) the compressed data simulation, 2) the matched filter on the residual, and 3) the thresholding for new estimation. Physically, this means that in every iteration of the ITA, the useful information in the residue (not the raw data) is first extracted by MF and then added to the current estimate to yield a new update; finally, the thresholding procedure enforces the sparsity through regularizing the noise and ambiguity from undersampling.

The algorithm stops when it converges or achieves the maximum number of iterations. For convenience of use, we list the pseudocode of ITA (25) as Algorithm 2. We further show how the parameters in (25) can be set adaptively.

[2]Although the sampling scheme on range may vary pulse by pulse, we still use this expression, which is easily understood

Algorithm 2: Iterative Thresholding Algorithm for Approximate Observation-Based CS-SAR Imaging

Require: SAR raw echoes $\mathbf{Y}_s$, approximated observation operator G and M, sampling operator $\mathbf{\Theta}_\eta, \mathbf{\Theta}_\tau$

Ensure: The recovery image $\mathbf{X}^*$

Initial: $\mathbf{X}^{(0)} = 0$,λ, μ and max iteration $I_{\max}$

1: **for** $i = 0$ to $I_{\max}$ **do**

2: Residue: $\tilde{\mathbf{R}}^{(i)} = \mathbf{Y}_s - \mathbf{\Theta}_\eta \mathrm{G}(\mathbf{X}^{(i)})\mathbf{\Theta}_\tau$

3: MF on residue:$\Delta\mathbf{X}^{(i)} = \mathrm{M}(\mathbf{\Theta}_\eta^T \mathbf{R}^{(i)} \mathbf{\Theta}_\tau^T)$

4: Thresholding: $\mathbf{X}^{(i+1)} = \mathrm{E}_{1,\lambda\mu}(\mathbf{X}^{(i)} + \mu\Delta\mathbf{X}^{(i)})$

5: **end for**

B. Parameter Setting

There are two parameters μ and λ in (25) that need to be set. First, μ controls convergence of the ITA that the inverse should obey:

$$0 < \mu^{-1} < \|\mathbf{A}\|_2^2. \tag{26}$$

However, it is difficult to calculate $\|\mathbf{\Theta}_\eta \mathrm{G} \mathbf{\Theta}_\tau\|_2^2$ directly, where operator G is included. As an alternative, we adopt the adaptive step selection strategy in [24] as

$$\mu_i = \left\| \mathbf{\Theta}_\eta \mathrm{G}\left(\Delta\mathbf{X}_k^{(i)}\right) \mathbf{\Theta}_\tau \right\|_F^2 \Big/ \left\| \Delta\mathbf{X}_k^{(i)} \right\|_F^2 \tag{27}$$

where $\Delta\mathbf{X}_k^{(i)}$ equals to $\Delta\mathbf{X}^{(i)}$ at the support of $\mathbf{X}^{(i-1)}$, and equal to zero elsewhere. It is easy to demonstrate that μ_i satisfies (27), and as reported in [24], such a choice has an additional advantage of accelerating the algorithm.

Further, the regularization parameter λ, which functions to compromise the reconstruction precision and the sparsity of the solutions obtained, has a substantial impact on the imaging result. Fortunately, as a part of the L_q regularization theory, the optimally λ has been resolved in [21], whenever the problem's sparsity is known. More precisely, assume the considered problem has sparsity k (i.e., a k-sparsity problem), then the optimal setting problem of parameter λ^* is shown to satisfy

$$\lambda^* \in \left[\left| b_\mu(\mathbf{x}^*) \right|_{k+1} / \mu, \left| b_\mu\left(\mathbf{x}^*\right|_k\right) / \mu \right] \tag{28}$$

where $b_\mu(\mathbf{x}) = \mathbf{x} + \mu\Delta\mathbf{x}$, $|b_\mu(\mathbf{x}^*)|_k$ is its kth largest component in magnitude.

Therefore, we suggest the setting that, in the nth iteration, $\lambda_i = |b_\mu(\mathbf{x}^{(i)})|_{k+1}/\mu_i$ ($\lambda_i\mu_i$ is independent of μ_i). The sparsity k, which determines λ_i, can be much more flexible to be set, say, based on a prior upper estimation on sparsity of the target scene.

C. Computation Cost

Let us compare the computational complexity and the memory occupation of the suggested CS-SAR imaging method (24), as compared with the known CS-SAR model (6). The purpose is to see how much reduction of computational cost of the new model has been brought. In the calculation, we have used some standard notations, which are the number of required iteration I, the sampling rate s, the number of range gates n_η, the number of range lines n_τ ($n = n_\tau \times n_\eta$), the number of samples of sent pulse u_τ, the number of samples of the synthetic aperture time u_η (they equal to the time bandwidth product (TBP) in each direction), and the TBP of radar signal $u = u_\eta \times u_\tau$.

With these notations, we can calculate the computational complexity of the approximate observation based CS-SAR C_a and the computational complexity of the exact observation based CS-SAR C_e, as follows. For C_a, it includes calculations of an inverse MF procedure and a MF procedure, which has commonly the computational complexity of $\mathcal{O}(n \log_2 n)$, together with a decoupled thresholding operator with complexity $\mathcal{O}(n)$ in a single step. Thus, the total cost is at the order $C_a = \mathcal{O}(In \log_2 n)$. For C_e, it includes calculations of a single iteration, two matrix multiplications and the thresholding procedure. Since there are only few nonzero entries in $\mathbf{H}$, say, nearly us in every column, when coding it using two-dimensional convolution, it needs at least $2uns$ complex multiplication. Thus, we find that the total cost is $C_e = \mathcal{O}(Iuns)$. Then, the ratio between C_e and C_o is given by r_C:

$$r_C = \mathcal{O}\left(\frac{us}{\log_2 n}\right). \tag{29}$$

It is seen from (29) that the ratio r_C depends linearly on the TBP of radar signal u. In SAR applications, the u is always designed very large (thousands even millions) to improve the reconstruction signal to noise ratio (SNR), which will bring very high computational cost of the time domain reconstruction method.

The memory loads of the approximate observation-based CS-SAR M_a and the memory loads of the exact observation-based CS-SAR M_e can be estimated in the subsequent way. For M_a, it contains only the storage of input, output, and several parameter matrices (i.e., azimuth matched filter, range matched filter, and the amount of migration in RDA), which is summed up to $\mathcal{O}(n)$ bytes memory occupation. For M_e, although no filters are stored, it needs additionally to store a sensing matrix, with the number of nonzero entries of uns. However, because the Doppler history with same range cells share the identical pattern, we only need to store an intact holistic pattern (the convolution kernel) for each range gate to achieve a compression, resulting in an additional memory occupation of $16un_\tau$ bytes (a complex number occupies 16 bytes of memory), as compared with M_a. This additional cost can be very large in spaceborne SAR systems. For example, when $u = 10^6$ and $n_\tau = 10^4$, it requires more than 100-GB memory to store the array. However, the memory cost of RDA is only a few hundred megabytes in the same condition. This will further hamper the application of time domain methods into practice.

Finally, the required number of iteration steps is difficult to compare analytically, but in practice, no obvious difference is observed.

D. Summary

From the analysis in the previous subsections, we can see that the suggested new model (24) and method (25) have constituted a more efficient CS-based SAR imaging method. While preserving CS features, the new method has the following exclusive advantages.

- *Lower computational cost*: Due to the use of approximated observation, the method only involves 1-D operations, which makes the imaging process extremely efficient. It has reduced the computational complexity of the existing exact observation-based method significantly, as shown in (29). Meanwhile, taking full advantages of the decoupled structure after approximating the observation, the proposed method can save the memory cost with a remarkable amount, which is sometimes of more significance.
- *Higher compatibility*: Benefitting from high efficiency, MF is currently the mainstream of SAR imaging studying and application. Hence, other than BP-like operations used in most existing CS-SAR algorithms, it is more natural and practical to incorporate MF-like procedures in CS-SAR. Fortunately, the proposed method is just one example that combine CS and MF together. It is much easier to be understood and implemented, especially when some parameters are given by Doppler features, for example, the Doppler center and Doppler FM rate. In particular, the new procedure can be seen as a successive iterative refinement of the well-known MF-based method, which makes the new method more consistent. As a result, the proposed model requires little modification of the existing SAR imaging algorithms, which makes the combination of MF and CS much simpler.

All these features make the suggested new CS-SAR imaging method more useful and efficient, and possible, in particular, to be applied in high-dimensional SAR applications.

V. Simulations and Applications

In this section, several simulations and applications are provided to demonstrate the effectiveness and efficiency of the proposed CS-SAR imaging method. For abbreviations, we denote by CSRDA the CS-SAR imaging method (24) with the approximated observation G acquired from the inverse of RDA, and by CSEO the CS-SAR method (6) with the exact observation $\mathbf{H}$.

We first conduct a series of simulations to compare the performance of the CSRDA method, the CSEO method, and the traditional RDA method in terms of reconstruction ability, reconstruction quality, and reconstruction cost. Then, we apply the CSRDA to some real SAR imaging tasks from RADARSAT-1, which then further demonstrates the outperformance of the suggested method.

The sampling scheme used in the simulations are specified as follows. In the azimuth direction, we employed random downsampling, realized by selecting random rows from the raw data $\mathbf{Y}$, with sampling rate s_a. In the range direction, we picked up random samples independently on each sampled echoes in azimuth, with sampling rate s_r. In addition, we keep the ratio between s_a and s_r as 1:5.[3]

Table I lists the primary SAR parameters used in both simulations and applications. All the experiments were conducted on a workstation of an 8-core 2.4-GHz CPU with 32G memory. The CSRDA was implemented in Matlab 2012a, while the CSEO using optimized convolution was implemented in C++ with parallel codes and careful array operations.

[3]The suggested sampling strategy was designed to comprehensively compare the reconstruction algorithms. The proposed model itself is adaptive to more complicated sampling schemes, for example, jitter sampling in the azimuth direction [12] and random demodulation [25] in the range direction.

TABLE I
Primary Parameter of SAR System and Geometry

Parameter	Simulation	RadarSat-1
Slant range of scene center(km)	20	1016.7
Effective radar velocity(m/s)	350	7062
Beam squint angle(rad)	0	0.06
Radar center frequency(MHz)	5000	5300
Pulse repetition frequency(Hz)	175	1256.98
Range FM rate(MHz/μs)	37.5	0.72135
Pulse duration(μs)	2	41.75
Sampling rate(MHz)	75	32.317

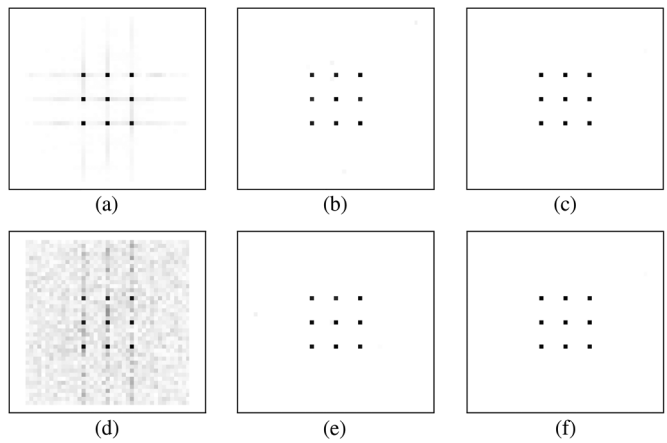

Fig. 3. Reconstruction results of nine point targets simulations with different sampling rate. From left to right are the reconstruction results of RDA, CSRDA, and CSEO, respectively, and the top row is with full samples while the bottom with 10% samples.

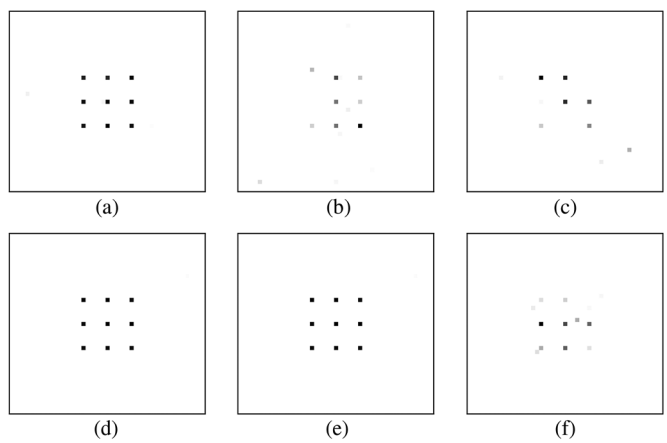

Fig. 4. Detailed comparison on needed least samples to reconstruct the image. The top row is the results from CSRDA, and the bottom row is from CSEO. From left to right are the results corresponding to the 0.65%, 0.55%, and 0.45% sampling rate, respectively.

A. Simulations

In the simulations, the scene was taken as 180×180, while the scattered coefficients were chosen with unit amplitude and uniform random phases. The raw data were first generated in time domain by exact slant range and then sampled with different rate to yield the compressed measurements. The sparsity parameter k was kept the same for CSRDA and CSEO, and the maximum iteration steps were set to 100 for both methods. The

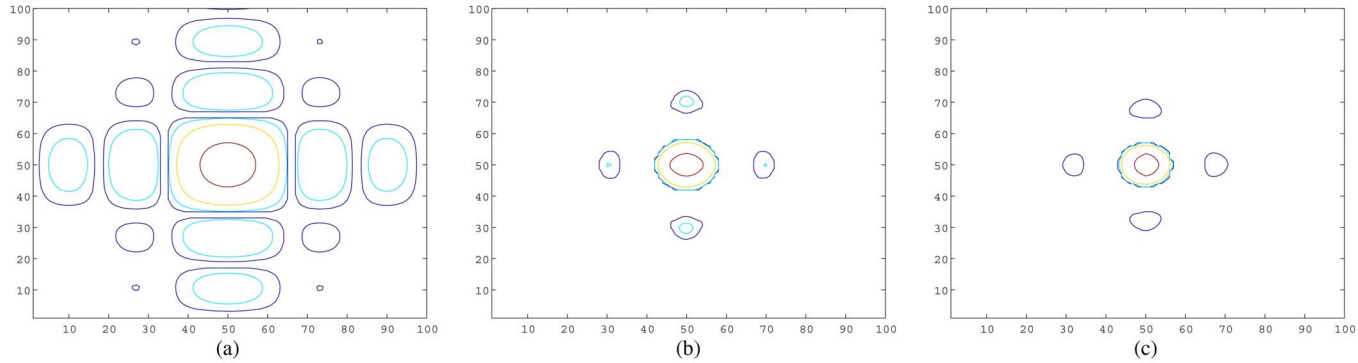

Method	PSLR(R)	PSLR(A)	IRW(R)	IRW(A)
RDA	-13.32 dB	-13.32 dB	15 samples	15 samples
CSRDA	-22.71 dB	-21.32 dB	8 samples	8 samples
CSEO	-26.73 dB	-25.02 dB	8 samples	8 samples

Fig. 5. Contours of magnitude. The red, yellow, light blue, and blue contour lines are corresponding to the value of -3 dB, -13 dB, -23 dB, and -33 dB. (a) Contours from RDA. (b) Contours from CSRDA. (c) Contours from CSEO.

aim of the simulations is then to compare the reconstruction ability (RA), reconstruction quality (RQ), and reconstruction cost (RC) of each competitive SAR imaging methods. These are measured, respectively, by the lowest amount of measurements by which a method can successfully reconstruct an image, the sidelobe and resolution of the reconstructed point target, and the computation time cost by a method to recover the image.

1) RA Comparison: A set of simulations was made where nine targets were located at the center with intervals of six samples. We varied the sampling rate ranged from 100% to 0.6% and added Gaussian noise with level of 20 dB. We applied RDA, CSRDA, and CSEO to this experiment with sparsity parameter $k = 18$. Some of the simulation results are shown in Figs. 3 and 4.

It is seen from the top row of Fig. 3 that with full samples (namely, with 100% sampling rate), all the methods RDA, CSEO, and CSRDA can successfully recover the scene, say, the amplitude of the target is maintained and no false target is observed. However, the reconstruction of RDA is with serious sidelobes, which is not observed in CSRDA and CSEO. This shows the exclusive advantage of the sparse regularization based CS-SAR imaging methodologies, as reported in [14]. When we reduce the sampling rate, say, 10% samples, as seen in the bottom of Fig. 3 RDA fails to recover the scene, while CSEO and CSRDA both can not only perfectly reconstruct the scene but also with significantly reduced sidelobes. In this case, no visible difference can be observed for CSEO and CSRDA. Nevertheless, when the sampling rate continues reducing as in Fig. 4, we found that both CSRDA and CSEO can reconstruct the image with only 0.65% of the samples. However, CSRDA fails with 0.55% samples while CSEO fails until the sampling rate takes 0.45%.

All the results consistently show that benefitting from sparse regularization, the approximate observation-based CS-SAR method can reconstruct sparse scenes with far less samples than Nyquist rate requires. However, caused by approximation, it requires slightly more samples to reconstruct the scene.

2) RQ Comparison: Sparse regularization was demonstrated in SAR and CS-SAR imaging the ability of reducing the sidelobe and simultaneously improving the resolving ability [14]. Hence, we are interested in whether the enhancement is kept when approximated observation is included, especially when the effect of the accuracy of the observation is excluded. To illustrate it, we compare the reconstruction quality of RDA, CSRDA, and CSEO in terms of sidelobe and spatial resolution, when successful reconstruction is achieved. The sidelobe is evaluated via the peak sidelobe ratio (PSLR), defined as the ratio of the peak intensity of the most prominent sidelobe to the peak intensity of the main lobe, i.e., the smaller the PSLR, the better an algorithm. The spatial resolution is measured by the impulse response width (IRW), defined as the width of the main lobe of the impulse response, measured by 3 dB below the peak value, or the minimum distance an algorithm can separate two targets, which should also be the smaller, the better. We have performed a one-point simulation with the upsampled factor 16 while the target is analyzed by a 16×16 chip centered on the peak, to yield a more detailed analysis on both the main lobe and the sidelobe. The sampling rate is fixed (20% for CSRDA and CSEO while 100% for RDA) to ensure a successful reconstruction. Since the recovery condition of the expanded sensing matrix is too bad, it is very difficult to achieve a perfect reconstruction. In contrast, we are interested in the RQ under a moderate regularization parameter; hence, the sparsity parameter k is set at 600. Some of the simulation results are given in Fig. 5.

Fig. 5 shows the contours of the reconstruction results, with contour lines of -3 dB (the boundary of main lobe) and -13 dB (the PSLR of traditional MF output). The comparison intuitively shows that both the area of the main lobe and the PSLR in the sidelobe reconstructed from CSRDA and CSEO are much smaller than those reconstructed from RDA. However, the difference between CSRDA and CSEO is still inconspicuous. Further in the table, details on the reconstruction quality are presented in azimuth and range directions. It is seen that the width of main lobe reconstructed from RDA is 15 samples both in range and azimuth, but for CSRDA and CSEO, the width is only 8 samples in the two directions. For the sidelobe, the PSLR reconstructed from the RDA is -13.32 dB in range and azimuth direction, which is very obvious. However, the CSRDA reduces the PSLR to -21.3 and -22.7 dB in azimuth and range, respectively, and the CSEO further reduces them to -25.0 and -26.7 dB, a little better than CSRDA.

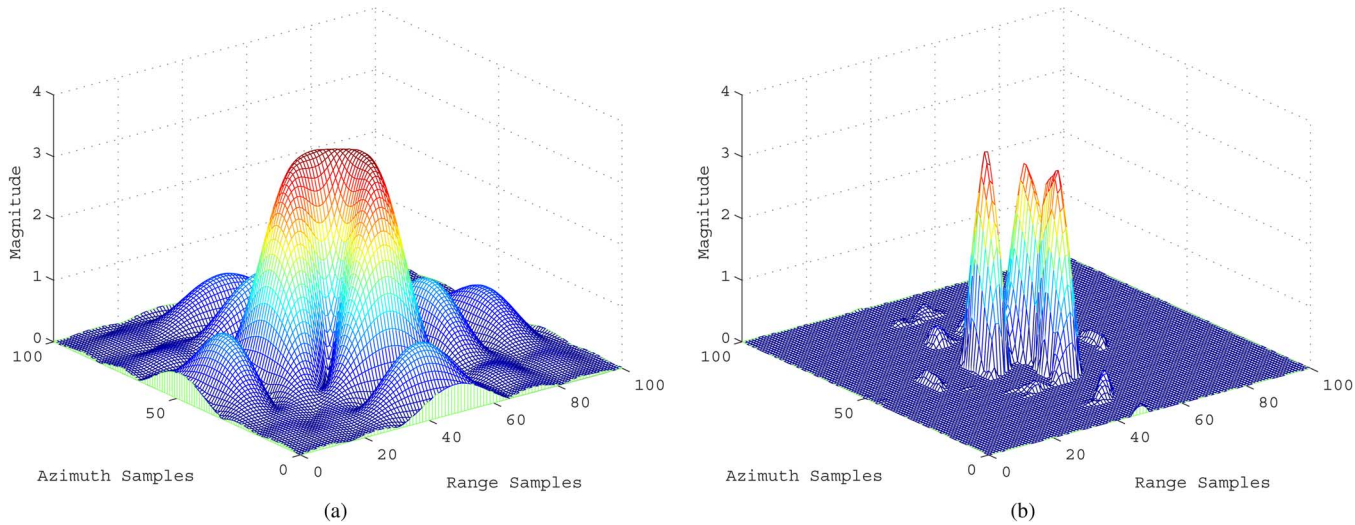

Fig. 6. Superresolution ability of the proposed method. (a) Result of RDA. (b) Result of CSRDA.

We further demonstrate the enhancement of resolution by CSRDA in another way. We add two point targets in the above simulation, with respectively azimuth and range intervals of 12 samples from the center. We then test whether the three targets can be separated from CSRDA. It is seen from the simulation result [Fig. 6(a)] that the reconstructed result of traditional RDA exhibits an overlapping of the main lobe; thus, the targets are inseparable. By using CSRDA in Fig. 6(b), one can clearly distinguish the locations of the three points, demonstrating an obvious enhancement of the resolution.

All of the simulations in this subsection demonstrate that by combining MF with sparse regularization, we can reduce the side lobe and improve the resolution simultaneously to a great extent. Note that these two goals have been regarded as tradeoffs traditionally, if only MF is employed.

3) RC Comparison: Finally, we compare the CPU time takes by CSRDA and CSEO. According to the analysis in Section IV, the computational complexity of CSRDA and CSEO depends on the scene size n and TBP of radar signal u. Therefore, we generated ten examples for each set of fixed scene size n and TBP of radar signal u in the simulation, with a constant sampling rate s 10%. The average computational time in a single iteration of the two methods was then recorded. The comparison results are shown in Fig. 7.

As we can observe from Fig. 7, when u is fixed as 10^5, the CSRDA scales very well to very high-dimensional problems, since even with $p = 10^7$, it only takes several second to finish an iteration. The CSEO is also insensitive to dimension when u is fixed. However, the CPU time of CSEO is consistently higher than that of CSRDA, with a ratio around 100. On the other hand, it is seen from Fig. 7(a) that when n is fixed to 10^7, the CPU time of CSRDA is constantly 3 s, but, the CPU time of CSEO depends linearly on u, which becomes more and more costly as u increases.

This RC comparison shows that the approximate observation-based CSRDA is much faster than the time-domain method CSEO, benefited from the $\mathcal{O}(n \log_2 n)$ computational cost of MF, and the computational complexity of CSEO depends linearly on both the TBP of radar pulse and the scene size. Therefore, when the u is large, i.e., 10^6, which is commonly in space-

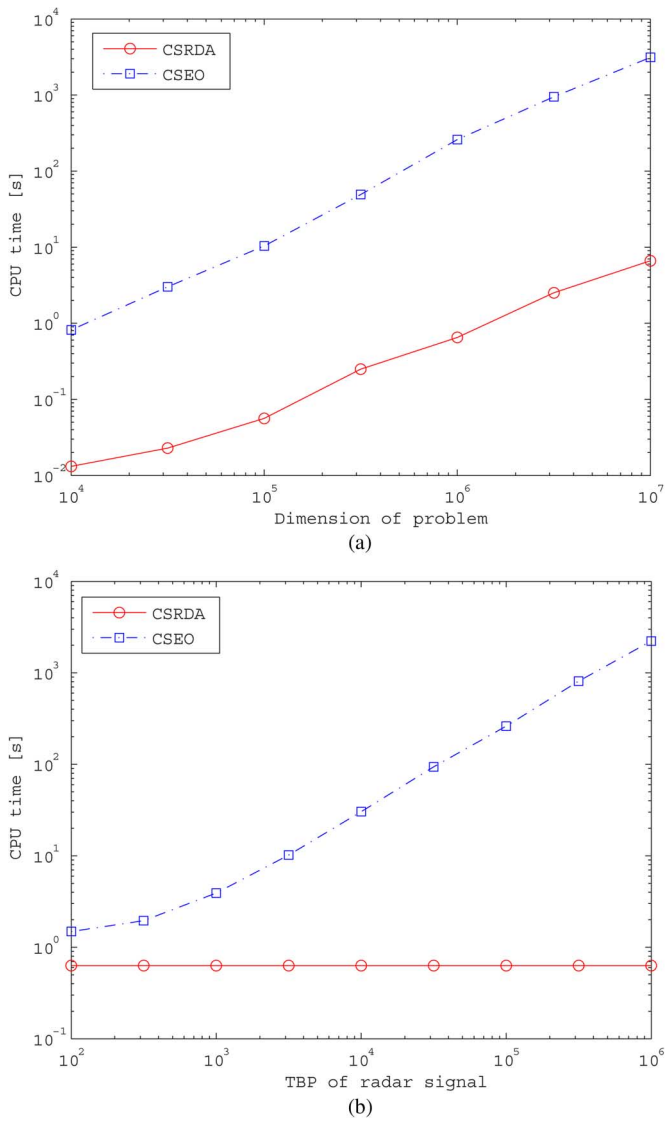

Fig. 7. CPU time of CSRDA and CSEO, where (a) u is fixed as 10^5. (b) p is fixed as 10^6.

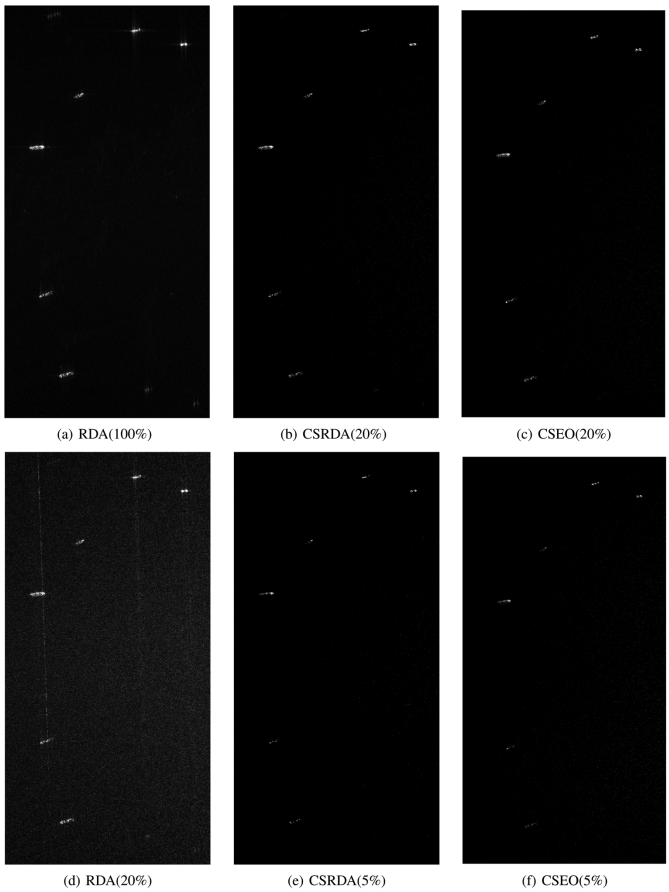

Fig. 8. Application on RADARSAT-1 (region of English Bay). (a) RDA with full samples. (b) CSRDA with 20% samples. (c) CSEO with 20% samples. (d) RDA with 20% samples. (e) CSRDA with 5% samples. (f) CSEO with 5% samples.

borne cases, CSRDA is expected to accelerate the CS-SAR reconstruction more than thousands of times. This acceleration of computational time together with the shown memory saving capacity demonstrate the superiority of the proposed method.

All the above simulations support that the suggested approximated observation-based CS-SAR method, CSRDA, is capable of high-quality imaging under Nyquist rates and with a comparable complexity as the traditional MF based imaging method. Especially, as compared with the exact observation-based CS-SAR imaging, CSRDA preserves the features of imaging under Nyquist rate and reconstruction with feature enhancement, while reducing the imaging complexity dramatically. Such significant complexity reduction property makes the new method applicable to large-scale imagery application (as will be demonstrated in the next subsection). This is, however, at the sacrifice of reconstruction quality or, equivalently, must be compensated with additional measurements. Thus, the new method provides a satisfying tradeoff between the reconstruction complexity and quality.

B. Application

We have applied the new method, CSRDA, along with RDA and CSEO, to some real SAR imaging tasks. RADARSAT-1 is a famous satellite SAR launched at 1995, and the data used in this application were collected on June 16, 2002 with Fine Beam 2 about Vancouver region. The related key parameters of SAR system are as in Table I.

We first applied the three methods to reconstruction of the region of English Bay, in which 6 vessels are sparsely distributed, a very typical sparse scene. The scene was digitalized as 1024 $\times$ 512 image with azimuth resolution 9 m and range resolution 6 m. We then reconstruct the image by the three imaging methods with sparsity $K = 10\,000$, and with varied sampling rates from 100% to 5%. Some typical results of reconstructions are shown in Fig. 8. As expected, the application shows a completely similar performance as that in the simulations. For example, Fig. 8(a) exhibits that RDA can only reconstruct the image when samples are fully adopted, but strong sidelobe is observed. When sampling rate is 20%, RDA fails with obvious ambiguities, but CSRDA and CSEO both can perfectly recover the image, with much reduced sidelobe. Fig. 8(c) and (f) then shows that when sampling rate is reduced to 5%, the reconstruction of CSEO is with slightly higher precision than that of CSRDA, though both can still recover the targets. On the other hand, as listed in Fig. 7, CSRDA exhibits its dominant advantage in computational cost as compared with CSEO. For example, the computation time of reconstruction, when 20% samples are used, by CSRDA is 1 minute, while by CSEO is about 9 hours. In addition, CSEO needs to store the sensing matrix which occupies about 16-Gb memory, while only 100 Mb for CSRDA.

We further applied the CSRDA to the large scale imaging problem together with RDA. However, the CSEO is not compared in this experiment because the memory cost is beyond the computational ability of our computer. The scene has a size 2048 $\times$ 2500 samples, which is of large scale but not so sparse. CSRDA can be applied in principle because sparse regularization, which is adopted in CS-SAR, can be used as a feature enhanced imaging method (with suppressed side lobe and improved resolution), as demonstrated in the simulations. The reconstruction results by RDA and CSRDA (with 100% sampling rate) are shown in Fig. 9. It is seen from Fig. 9 that CSRDA has resulted the reconstruction with improved resolution and reduced sidelobes, as demonstrated in the zoomed Fig. 10.

The applications above support that the suggested approximated observation based CS-SAR imaging is effective and efficient, especially applicable to high-dimensional SAR imaging applications. Such benefit clearly improves on the currently used exact observation based CS-SAR imaging methods.

VI. Conclusion

Compressed sensing (CS) has been applied to yield novel SAR imaging methodologies under Nyquist sampling in recent years. The resultant CS-SAR models are time domain based and using the exact observation, which then makes it of very high computational cost, and is difficult to be applied in high-dimensional applications. In this paper, we have proposed an approximated observation and frequency-domain-based CS-SAR imaging method, with which the computational complexity can be dramatically reduced.

The main contributions of the present work are as follows.

i) Instead of the exact observation matrix, an operator, called the approximated observation, is constructed to generate SAR raw data by means of inverse of any traditional MF-based imaging procedure (like RDA).

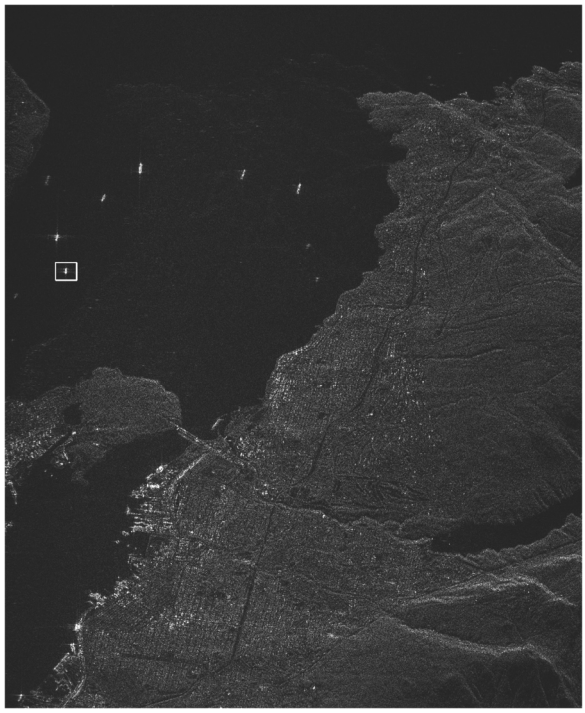

(a)

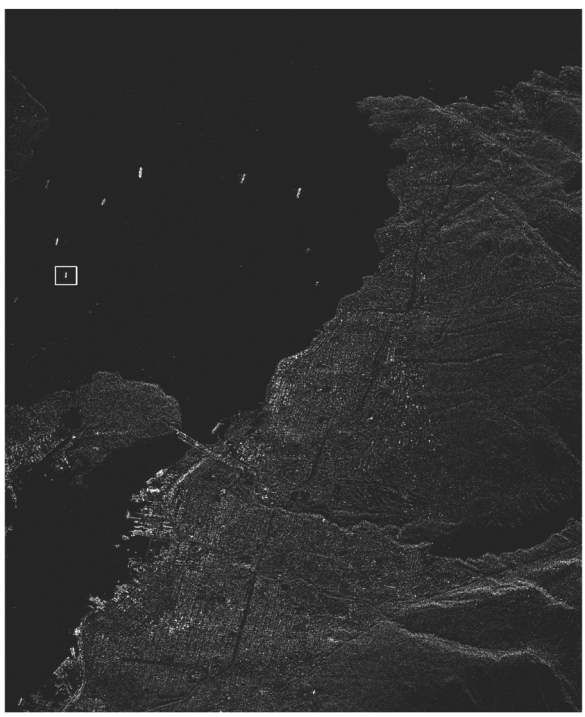

(b)

Fig. 9. Application results on RADARSAT-1. (a) RDA with full samples. (b) CSRDA with full samples.

Such generic construction makes the SAR imaging approximately decoupled, very fast in processing, while naturally connecting the existing MF-based SAR imaging algorithms.

ii) Incorporating the approximated observation into CS-SAR framework, an efficient sparse regularization based CS-SAR model is formulated. The new model combines naturally CS and MF and is compatible with most existing SAR imaging methods, which needs a little modification of the current SAR imaging technologies.

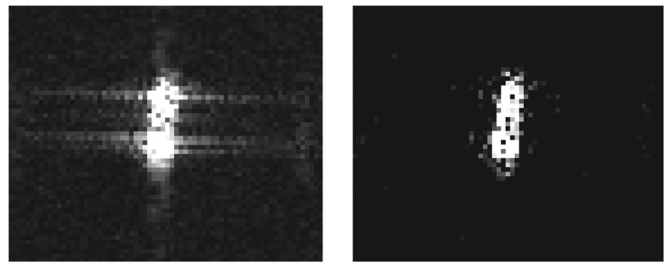

(a) (b)

Fig. 10. Detailed comparison on the selected area with enlarged scale. (a) RDA. (b) CSRDA.

iii) With the use of approximated observation, an iterative thresholding algorithm is suggested for fast solution of the new CS-SAR model, which forms a low complexity, CS featured, new SAR imaging method.

We have tested and applied the new suggested CS-SAR method with a series of simulations and applications. The experiments consistently support that the new method is capable of reconstructing sparse scenes with far fewer measurements than Nyquist requires, yielding always a feature enhanced high-quality imaging and bringing a speed-up of reconstruction hundreds of times as compared with the exact observation-based CS-SAR methods. Due to the fast and feature enhancement features, the new CS-SAR method can be accepted as an efficient CS type SAR imaging technique, especially for high-dimensional imaging applications.

It is worthwhile, however, to remark that although significant complexity reduction (speed-up of reconstruction) can be brought, the use of the approximated observation requires more samples to reconstruct a scene. Thus, how and to what extent the approximation does affect the reconstruction deserves a further study. Moreover, since there are many possibilities of concrete realizations of the approximated observation, the criterion on how to select an appropriate one deserved study.

Further, although the proposed method provides a fast implementation of CS-SAR, it does not overcome the essential limitations of CS-SAR. On one hand, the sparsity of scene, which is the prerequisite of CS, could not be strictly defined. Even in some specific conditions that the strong targets are dominant, for example in Fig. 8, there are still many trivial targets in the dark background. In practice, however, we assume them as zeros. As a result, CS algorithms, either greedy or ITA, always kill such small scatterers and affect more or less the understanding of reconstructed image and some applications. On the other hand, the existing subsampling strategy for CS-SAR may not ensure a desired recovery condition so that there always requires much more samples than what essentially requires.

All those problems are under our current research.

REFERENCES

[1] I. G. Cumming, M. Dettwiler and Associates Staff, and F. H. Wong, *Digital Signal Processing of Synthetic Aperture Radar Data: Algorithms and Implementation*. Norwood, MA, USA: Artech House, 2004.

[2] E. J. Candès, "Compressive sampling," in *Proc. Int. Congr. Math.*, 2006, pp. 1433–1452.

[3] R. G. Baraniuk, "Compressive sensing," *IEEE Signal Process. Mag.*, vol. 24, no. 4, pp. 118–121, 2007.

[4] D. L. Donoho, "Compressed sensing," *IEEE Trans. Inf. Theory*, vol. 52, no. 4, pp. 1289–1306, 2006.
[5] A. C. Gurbuz, J. H. McClellan, and W. R. Scott, Jr., "Compressive sensing for subsurface imaging using ground penetrating radar," *Signal Process.*, vol. 89, no. 10, pp. 1959–1972, 2009.
[6] M. A. Herman and T. Strohmer, "High-resolution radar via compressed sensing," *IEEE Trans. Signal Process.*, vol. 57, no. 6, pp. 2275–2284, 2009.
[7] J. H. G. Ender, "On compressive sensing applied to radar," *Signal Process.*, vol. 90, no. 5, pp. 1402–1414, 2010.
[8] L. C. Potter, E. Ertin, J. T. Parker, and M. Cetin, "Sparsity and compressed sensing in radar imaging," *Proc. IEEE*, vol. 98, no. 6, pp. 1006–1020, 2010.
[9] S. Bhattacharya, T. Blumensath, B. Mulgrew, and M. Davies, "Fast encoding of synthetic aperture radar raw data using compressed sensing," in *IEEE/SP 14th Workshop Statist. Signal Process.*, 2007, pp. 448–452.
[10] G. Rilling, M. Davies, and B. Mulgrew, "Compressed sensing based compression of SAR raw data," in *Proc. Signal Process. Adapt. Sparse Structured Represent. (SPARS'09)*, 2009.
[11] M. Tello Alonso, P. López-Dekker, and J. J. Mallorqui, "A novel strategy for radar imaging based on compressive sensing," *IEEE Trans. Geosci. Remote Sens.*, vol. 48, no. 12, pp. 4285–4295, 2010.
[12] V. M. Patel, G. R. Easley, D. M. Healy, and R. Chellappa, "Compressed synthetic aperture radar," *IEEE J. Sel. Topics Signal Process.*, vol. 4, no. 2, pp. 244–254, 2010.
[13] J. S. Zeng, J. Fang, and Z. B. Xu, "Sparse SAR based on $L_{1/2}$ regularization," *Sci. China Inf. Sci.*, vol. 55, no. 8, pp. 1755–1775, 2012.
[14] M. Çetin and W. C. Karl, "Feature-enhanced synthetic aperture radar image formation based on nonquadratic regularization," *IEEE Trans. Image Process.*, vol. 10, no. 4, pp. 623–631, 2001.
[15] A. S. Khwaja, L. Ferro-Famil, and E. Pottier, "SAR raw data simulation using high precision focusing methods," in *Proc. Eur. Radar Conf. (EuRAD)*, 2005, pp. 33–36.
[16] G. Franceschetti, R. Guida, A. Iodice, D. Riccio, and G. Ruello, "Efficient simulation of hybrid stripmap/spotlight SAR raw signals from extended scenes," *IEEE Trans. Geosci. Remote Sens.*, vol. 42, no. 11, pp. 2385–2396, 2004.
[17] C. Wu, K. Y. Liu, and M. Jin, "Modeling and a correlation algorithm for spaceborne SAR signals," *IEEE Trans. Aerosp. Electron. Syst.*, no. 5, pp. 563–575, 1982.
[18] S. J. Wei, X. L. Zhang, J. Shi, and G. Xiang, "Sparse reconstruction for SAR imaging based on compressed sensing," *Progr. Electromagn. Res.*, vol. 109, pp. 63–81, 2010.
[19] E. J. Candès, J. Romberg, and T. Tao, "Robust uncertainty principles: Exact signal reconstruction from highly incomplete frequency information," *IEEE Trans. Inf. Theory*, vol. 52, no. 2, pp. 489–509, 2006.
[20] I. Daubechies, M. Defrise, and C. De Mol, "An iterative thresholding algorithm for linear inverse problems with a sparsity constraint," *Commun. Pure Appl. Math.*, vol. 57, no. 11, pp. 1413–1457, 2004.
[21] Z. B. Xu, X. Y. Chang, F. M. Xu, and H. Zhang, "$L_1/2$ regularization: A thresholding representation theory and a fast solver," *IEEE Trans. Neural Netw. Learn. Syst.*, vol. 23, no. 7, pp. 1013–1027, 2012.
[22] T. Blumensath and M. E. Davies, "Iterative hard thresholding for compressed sensing," *Appl. Comput. Harmon. Anal.*, vol. 27, no. 3, pp. 265–274, 2009.
[23] C. Wu, "A digital system to produce imagery from SAR data," *Syst. Design Driven by Sensors*, vol. 1, 1976.
[24] T. Blumensath and M. E. Davies, "Normalized iterative hard thresholding: Guaranteed stability and performance," *IEEE J. Sel. Topics Signal Process.*, vol. 4, no. 2, pp. 298–309, 2010.
[25] J. A. Tropp, J. N. Laska, M. F. Duarte, J. K. Romberg, and R. G. Baraniuk, "Beyond Nyquist: Efficient sampling of sparse bandlimited signals," *IEEE Trans. Inf. Theory*, vol. 56, no. 1, pp. 520–544, 2010.

Jian Fang (S'12) was born in Jiangsu, China, in 1986. He received the B.Sc. degree in mathematics from Nanjing Normal University, Nanjing, China, in 2008.

He is currently working towards the Ph.D. degree with the School of Mathematics and Statistics, Xi'an Jiaotong University, Xi'an, China. His research interests include sparse modeling and synthetic aperture radar imaging.

Zongben Xu received the Ph.D. degree in mathematics from Xi'an Jiaotong University, Xi'an, China, in 1987.

He currently serves as a Vice-President with Xi'an Jiaotong University, the Academician of the Chinese Academy of Sciences, the Chief Scientist of the National Basic Research Program of China (973 Project), and the Director of the Institute for Information and System Sciences of the University. His current research interests include nonlinear functional analysis and intelligent information processing.

Dr. Xu was a recipient of the National Natural Science Award of China in 2007 and was a winner of the CSIAM Su Buchin Applied Mathematics Prize in 2008. He delivered a talk at the International Congress of Mathematicians 2010.

Bingchen Zhang received the M.S. degree from the Institute of Electronics of Chinese Academy of Science, Beijing, China, in 1999.

He currently serves as a scientist in the Institute of Electronics, Chinese Academy of Sciences, Beijing, China. His research interests consist of signal and information processing, remote sensing technology, and sparse signal processing.

Wen Hong (M'03) was born in Shanxi, China, in 1968. She received the M.S. degree from Northwestern Polytechnical University, Xi'an, China, in 1993 and the Ph.D. degree from the Beijing University of Aeronautics and Astronautics (BUAA), Beijing, China, in 1997.

She was formerly a Faculty Member in signal and information processing with the Department of Electrical Engineering, BUAA. She worked as a Guest Scientist for one year with the German Aerospace Center (DLR), Wessling, Germany. Since 2002, she has been with the National Key Laboratory of Microwave Imaging Technology, Institute of Electronics, Chinese Academy of Sciences, Beijing, China, as a Scientist and a Supervisor of the graduate student program. Her research interests include synthetic aperture radar imaging and its applications.

Yirong Wu (M'00) received the Ms.D. degree from the Beijing Institute of Technology, Beijing, China, in 1988 and the Ph.D. degree from the Institute of Electronics, Chinese Academy of Sciences (IECAS), Beijing, China, in 2001.

Since 1988, he has been with IECAS, where he is currently the Director. He has over 20 years of experience in remote sensing processing system design. His current research interests are microwave imaging, signal and information procession, and related applications.